

Supplemental Information

Methods

PCR primers for mice genotyping

The *Gab1^{fllox}* allele can be distinguished from the wild type *Gab1* allele by PCR on genomic DNAs extracted from tails, using the primer pair

5'-GCGCCTTCTTTGCATCACCTCATCT-3' and

5'-GGTAAAGCAGGTCTAGGTGGCTGACAGTCT-3'. *Cre*-transgene allele was detected

by PCR using the primers; 5'-ACATG TTCAGGGATCGCCAG-3' and

5'-TAACCAGTGAAACAGCATTGC-3'. *Gab2* allele was determined by PCR using the

following primers: 5'-AATGTAGACAGTCAGTGCCTAGAGGGTCCA-3' and 5'-

CATGTATCATGACATTTGTGCTCCACCA-3' for wild type allele detection;

5'-AATGTAGACAGTCAGTGCCTAGAGGGTCCA-3' and

5'-CAGCAGCCTCTGTTCCACATACTTCAT-3' for deleted allele detection.

Materials. Anti-caspase-3, and anti-cleaved caspase-3 (Asp175) Ab were purchased from Cell Signaling Technology. Anti-ErbB1, ErbB2 (Neu), ErbB3, and ErbB4 Ab were from Santa Cruz Biotechnology. Hoechst33342 and staurosporine were from Sigma. VEGF was from R&D.

RT-PCR analyses. Total RNAs extracted from heart tissues were subjected to RT-PCR using Superscript II, a reverse transcriptase, and random hexamers (Invitrogen). The first strand cDNAs were PCR-amplified, using the following primer pairs: *Gab1*

5'-ATGAGCGGCGGCGAAGTGGTTTGCT-3' and
5'-CGCGACTGAAGAAGCTTCCATCTGA-3'; Gab2
5'-GAGAAGAAGTTGAGGCGCTA-3' and 5'-TGGACCCACTTATTCATGTC -3'; Gab3
5'-GAGAGTCTCTCTCACATGC-3' and 5'-GGGTGAAGCTGTGGGATA-3' ; GAPDH
5'-TGAAGGTCGGAGTCAACGGATTTGG-3' and
5'-CATGTGGGCCATGAGGTCCACCAC-3'(Wolf et al., 2002).

Mouse strains. The transgenic mice expressing the Cre recombinase under the control of α -MHC promoter in C57BL/6J background (α -MHC-Cre mice) were generated as previously reported (Yamaguchi et al., 2004). To examine the spatio-temporal recombination mediated by α -MHC promoter-driven Cre, α -MHC-Cre mice were crossed with enhanced green fluorescent protein (EGFP) reporter mice (CAG-CAT-EGFP) obtained from J. Miyazaki, Osaka University).(Kawamoto et al., 2001)

Histological analyses. Hearts from mice at indicated age were fixed with 10% neutralized formalin, embedded in paraffin, and sectioned at 4 μ m thickness. H&E, Masson's trichrome and Elastica van Gieson stainings were performed on serial sections. For electron microscopy, LV from mice at 12 wk of age were fixed with 2.5% glutaraldehyde in 0.1 M phosphate buffer (pH 7.4), sectioned and stained by the conventional osmium-uranium-lead method. For the terminal deoxyribonucleotidyl transferase-mediated dUTP-biotin nick end labeling (TUNEL) assay, the hearts were resected, embedded in OCT compound (SAKURA), frozen, and cryosectioned perpendicular to the long axis. We performed

TUNEL assay using in situ cell death detection kit (Roche) according to the manufacturer's instructions. Sections were co-stained with Hoechst33342. The number of TUNEL-positive nuclei was counted by examining the entire section with a $\times 40$ objective.

Molecular mass spectrometric analyses. Heart lysates from control (flox/flox) and Gab1CKO mice at 10 wk of age were immunoprecipitated using anti-Gab1 serum, followed by silver staining and immunoblotting with anti-Gab1 Ab. The bands, which were detected in the immunoprecipitates of control mice but not in those of Gab1CKO mice heart lysates, were excised from the silver-stained gel and subjected to mass spectrometry. Mass spectrometric identification of proteins was performed as previously described (Jensen et al., 1996). Briefly, after SDS-PAGE, the proteins visualized by silver staining were excised separately from gels, followed by the in-gel digestions with trypsin (Promega) in a buffer containing 50 mM ammonium bicarbonate (pH 8.0) and 2% acetonitrile overnight at 37°C. Molecular mass analyses of tryptic peptides were performed by matrix-assisted laser desorption/ionization time-of-flight mass spectrometry (MALDI-TOF/MS) using an ultraflex TOF/TOF (Bruker Daltonics). Proteins were identified by comparison between the MW determined by MALDI-TOF/MS and theoretical peptides masses from Gab1.

Isolation of cardiomyocytes and non-cardiomyocytes. After Percoll-gradient isolation of cardiomyocytes and non-cardiomyocytes from neonatal rat hearts, we characterized non-cardiomyocytes by immunostaining these cells using following antibodies; anti- α -SMA monoclonal antibody (for smooth muscle staining, DAKO), anti-vWF

polyclonal antibody (for endothelia cell staining, DAKO). The population of non-cardiomyocytes were as follows; α -SMA-positive smooth muscle cells (5.2%), vWF-positive endothelial cells (8.7%), α -actinin-positive cardiomyocytes (1.0%). The residual cells in this fraction (approximately 85%) might be ascribed to cardiac fibroblasts.

Statistical analysis. All data were expressed as mean \pm SEM. Differences among multiple groups were compared by one-way ANOVA followed by a post hoc comparison tested with Scheffe's method. Student's *t*-test was used to analyze differences between two groups. A value of $P < 0.05$ was considered as statistically significant.

References

Jensen,O.N., Podtelejnikov,A., and Mann,M. (1996). Delayed extraction improves specificity in database searches by matrix-assisted laser desorption/ionization peptide maps. *Rapid Commun. Mass Spectrom.* *10*, 1371-1378.

Kawamoto,S., Nitta,Y., Tashiro,F., Nakano,A., Yamato,E., Tahara,H., Tabayashi,K., and Miyazaki,J. (2001). Suppression of T(h)1 cell activation and prevention of autoimmune diabetes in NOD mice by local expression of viral IL-10. *Int. Immunol.* *13*, 685-694.

Wolf,I., Jenkins,B.J., Liu,Y., Seiffert,M., Custodio,J.M., Young,P., and Rohrschneider,L.R. (2002). Gab3, a new DOS/Gab family member, facilitates macrophage differentiation. *Mol. Cell Biol.* *22*, 231-244.

Yamaguchi,O., Watanabe,T., Nishida,K., Kashiwase,K., Higuchi,Y., Takeda,T., Hikoso,S., Hirotani,S., Asahi,M., Taniike,M., Nakai,A., Tsujimoto,I., Matsumura,Y., Miyazaki,J., Chien,K.R., Matsuzawa,A., Sadamitsu,C., Ichijo,H., Baccarini,M., Hori,M., and Otsu,K. (2004). Cardiac-specific disruption of the c-raf-1 gene induces cardiac dysfunction and apoptosis. *J. Clin. Invest* *114*, 937-943.

Supplemental Figure Legends

Supplemental Figure 1 RT-PCR shows the expression of Gab1 and Gab2 mRNAs, but not Gab3 mRNA in the murine heart.

Supplemental Figure 2 Molecular characterization of high MW Gab1 isoform in the heart.

(A) Heart lysates from control (flox/flox) and Gab1CKO mice were subjected to immunoprecipitation with anti-Gab1 serum, followed by silver staining and immunoblotting with anti-Gab1 Ab. The bands, which were detected in the immunoprecipitates of control mice but not in those of Gab1CKO mice heart lysates were excised from silver-stained gel and subjected to mass spectrometry. The Band 1 in the left panel corresponded to the high MW Gab1 and the Band 2 in the left panel corresponded to the low MW Gab1 which was reduced to approximately 20% in Gab1CKO mice heart. (B) The result of TOF-MS using the fragments obtained by A. The amino acid sequence of murine Gab1 (gi46396021) is written in black characters. The underlined peptides were identified by a mass spectrometry analysis of Band 1. The peptides marked by red characters were identified by a mass spectrometry analysis of Band 2. (C) Band 1 corresponding to the high MW Gab1 was confirmed to possess the partial amino acid sequence of Gab1. Top panel and bottom panel show the peptide fragments and their molecular weights obtained from the mass analysis of Band 1 and Band 2, respectively. (D) Cardiac-specific high MW Gab1 was detected in neonatal rat cardiomyocytes (CM), but not in neonatal rat non-cardiomyocytes (non-CM). Cell lysates from two independent experiments were analyzed. AKT was checked as a loading control. Arrows indicate two

isoforms of Gab1 in CM.

Supplemental Figure 3 Tyrosine-phosphorylation of ErbB receptors in the murine hearts upon stimulation with NRG-1 β . Receptor tyrosine-phosphorylation was examined by IB using PY99 Ab after IP with anti-ErbB1 Ab (**A**), anti-ErbB2 Ab (**B**), anti-ErbB3 Ab (**C**), or anti-ErbB4 Ab (**D**). Note that ErbB2 and ErbB4 were strongly tyrosine-phosphorylated after injection with NRG-1 β . (**E**) Co-IP of Gab1 with ErbB4 after stimulation with NRG-1 β was observed in the heart lysate of mice stimulated with NRG-1 β for 5 min. Representative blots of three experiments are shown.

Supplemental Figure 4 Spatio-temporal Cre-mediated recombination in the embryos of α -MHC-Cre transgenic mice and ablation of Gab1 protein during the various postnatal stages of Gab1CKO mice. (**A**) α -MHC-Cre mice were bred with enhanced green fluorescent protein (EGFP) reporter mice (CAG-CAT-EGFP mice). We observed strong expression of EGFP in the hearts of offsprings which possessed both α -MHC-Cre and CAG-CAT-EGFP allele (denoted as α -MHC/EGFP) at embryonic day 10.5 (E10.5) and 14.5 (E14.5). (**B**) To examine whether Gab1 protein is efficiently ablated during postnatal development in Gab1CKO mice, we investigated Gab1 expression by performing western blot analyses using heart lysates from control (flox/flox) and Gab1CKO mice at the indicated age. We observed the ablation of Gab1 protein even in the hearts of 3 d-old Gab1CKO mice as well as 3 wk- and 10 wk-old Gab1CKO. SHP2 was checked as a loading control. Arrows indicate two isoforms of Gab1 in the hearts.

Supplemental Figure 5 DKO mice displayed progressive ventricular dilatation during postnatal development. **(A)** Elastica van Gieson staining of heart sections from flox/flox, Gab1CKO, Gab2KO and DKO mice at birth showed neither difference in heart size nor accumulation of elastic fibers. Scale bars, 500 μm . **(B)** Representative images of Elastica van Gieson staining of heart sections from four groups of mice at approximately d 300 of age. The right panel shows the remarkably dilated heart section from DKO mice which died at d 304 presumably of heart failure. We could not observe any difference of heart size and histology among other three groups of mice including flox/flox, Gab1CKO and Gab2KO. Scale bar, 1 mm.

Supplemental Figure 6 DKO mice did not show any obvious interstitial fibrosis in the left ventricles. **(A)** H&E-stained sections of myocardium beneath the epicardium from each group of mice. **(B)** Masson's trichrome-stained sections of myocardium beneath the epicardium from each group of mice. DKO mice did not show interstitial fibrosis in the left ventricles. Scale bars 20 μm (**A** and **B**).

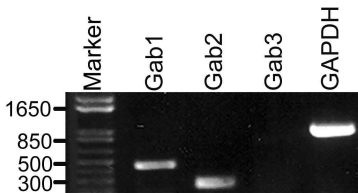
Supplemental Figure 7 Apoptotic analyses and electron microscopic analyses of DKO mice hearts. **(A)** TUNEL assays in the hearts of control (flox/flox) and DKO mice (n=4, each group). No significant change in the number of TUNEL-positive nuclei was observed. **(B)** Caspase-3 was not activated in the hearts of DKO mice as well as in those of control mice. Heart lysates from control (flox/flox) and DKO mice were subjected to

immunoblotting with anti-caspase-3 and anti-cleaved caspase-3 Ab. Arrows denotes the position of caspase-3 and cleaved-caspase-3. As a positive control, we used the cell lysate of HUVECs which were treated with 1 μ M staurosporine (STS) for 3 h. **(C)** Electron microscopic analysis of myofibrillar architecture in the ventricles of control (flox/flox) and DKO mice at 12 wk of age. Marked reduction of sarcomere length was observed in DKO myofibrils, suggesting the hypercontraction of the myocardium. Arrows indicate adjacent Z-lines. Scale bars, 1 μ m. **(D)** Electron microscopic analysis of mitochondria in the ventricles of control (flox/flox) and DKO mice at 12 wk of age. Slightly swelled mitochondria with a little coarse structural changes of crista were observed in the LV of DKO mice. Scale bars, 0.5 μ m.

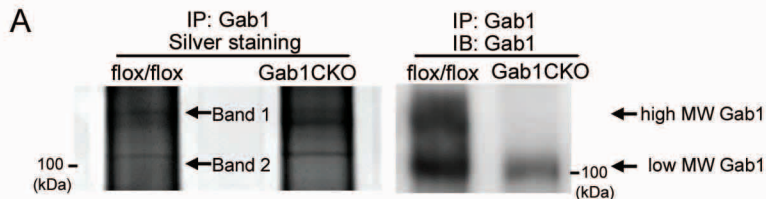
Supplemental Figure 8 DKO mice displayed progressive ventricular dilatation and contractile deterioration during postnatal development. **(A)** Left ventricular end diastolic diameter (LVEDD) of control (flox/flox) mice ($n=5$) and DKO mice ($n=5$) at indicated weeks was assessed by echocardiography. **(B)** Similar to **A**, fractional shortening (%FS) was examined by echocardiography. Note that DKO mice displayed progressive ventricular dilatation in parallel with reduction of contractility. There was no significant change between two groups at 3 wk. * $P<0.05$ and ** $P<0.01$ between the indicated groups, by one-way ANOVA.

Supplemental Figure 9 HB-EGF or IGF-1-induced activation of ERK and AKT was preserved in DKO mice. **(A)** HB-EGF-induced phosphorylation of both ERK and AKT was

assessed using phospho-specific antibodies. Control (flox/flox) or DKO mice were injected with 5 μ g of HB-EGF via inferior vena cava. The hearts were isolated at 5 min after injection. Activation of ERK and AKT was not attenuated in DKO heart compared to control heart. Representative blots of three independent experiments are shown. **(B)** IGF-1-stimulated activation of ERK and AKT was assessed using phospho-specific antibodies similarly to **A**. Heart lysates were prepared from control (flox/flox) or DKO mice injected with 5 μ g of IGF-1 via inferior vena cava. Phosphorylation of ERK and AKT was not attenuated in DKO heart compared to control heart. Representative blots of three independent experiments are shown.



Supplemental Figure1 Nakaoka et al.



B

1 MSGGEVVCSG WLRKSPPEKK LKRYAWKRRW FVLRSGRLTG **DPDVLEY**YKN
 51 DHAKKPIR **II DLNLCQQVDA GLTFNKKEFE NSYIFDINTI DRI**FYLVADS
 101 EEDMNKVVRC ICDICGFNPT EEDPVKPLTG SSQAPVDSPF AISTAPASSQ
 151 MEASSVALPP PYQVISLPPH PDTLGLQDDP QDYLLINCQ SKKPEPNRTL
 201 FDSA KPTFSE TDCNDNVP SH QTPASSQSKH GMNGFFQQM MYDCPPSR **LT**
 251 **SVSGESSLYN LPR**SYSHDVL PKE**SPS**STEA DGELYTFNTP SGTAGVETQM
 301 **RHVSISYDIP PTPGNTYQIP R**TFPESTLGQ SSK **LDTIPDI PPPRPPKPHP**
 351 **THDR**SPVETC GVPRTASD TD SSYCIPPPAG MTPSRNTIS TVDLNKLKRD
 401 ASSQDCYDIP RTFPSDR **SSS LEGFHSQYKI** KSVLTAGGVS GEELDENYVP
 451 MNPNSPPRQH SGSFTEPIQE PNYVPMPTGT FDFSSFGMQV PPPAHMGFRS
 501 SPKTPPR **RPV PVADCEPPV DR**NLKPDRK **V KPAPLDIKPL SEWEELOAPV**
 551 **R**SPITRSFAR DSSRFPMSPR PDSVHSTSS SDSHDSEENY VPMNPNLSGE
 601 DPNLFASNSL DGGSSPMNKP KGDQVEYLD LDLDSGKSTP PRKQKSSGSG
 651 SSMADERVDY VVVDQKTLA LKSTREAWTD GRQSTESETP TKNVK

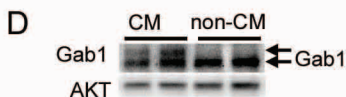
C

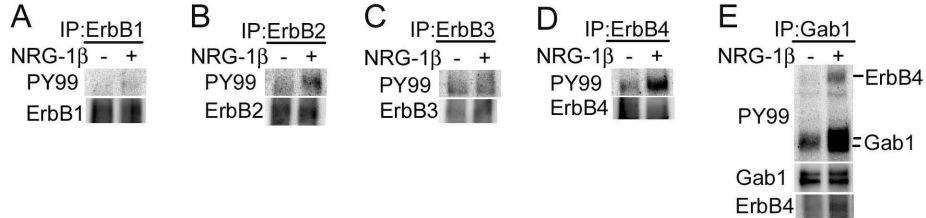
Band 1

Start - End	Observed	Sequence
249 - 263	1622.82	<u>LTSVSGESSLYNLPR</u>
78 - 92	1875.92	<u>EFENSYIFDINTIDR</u>
59 - 77	2133.09	<u>IIDLNLCQQVDAGLTFNKK</u>
302 - 321	2255.13	<u>HVSISYDIPPTPGNTYQIPR</u>
334 - 354	2396.19	<u>LDTIPDIPPPRPPKPHPTHDR</u>
530 - 551	2515.39	<u>VKPAPLDIKPLSEWEELOAPVR</u>

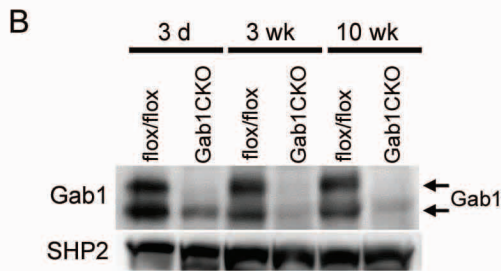
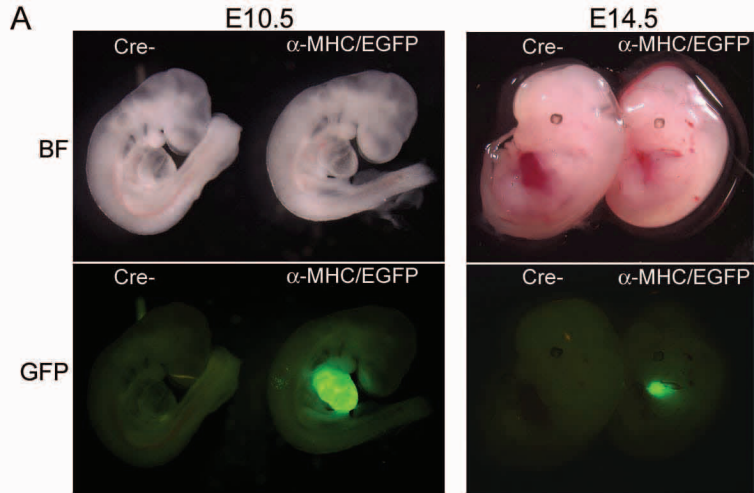
Band 2

Start - End	Observed	Sequence
418 - 429	1369.68	SSSLEGFHSQYK
38 - 49	1412.72	LTGDPDVLEYK
249 - 263	1622.76	LTSVSGESSLYNLPR
508 - 522	1646.82	RPVPVADCEPPVDR
78 - 92	1875.87	EFENSYIFDINTIDR
59 - 76	2005.08	IIDLNLCQQVDAGLTFNK
59 - 77	2133.12	IIDLNLCQQVDAGLTFNKK
302 - 321	2255.15	HVSISYDIPPTPGNTYQIPR
334 - 354	2396.27	LDTIPDIPPPRPPKPHPTHDR
530 - 551	2515.39	VKPAPLDIKPLSEWEELOAPVR
273 - 301	3062.36	ESPSSTEADGELYTFNTPSGTAGVETQMR

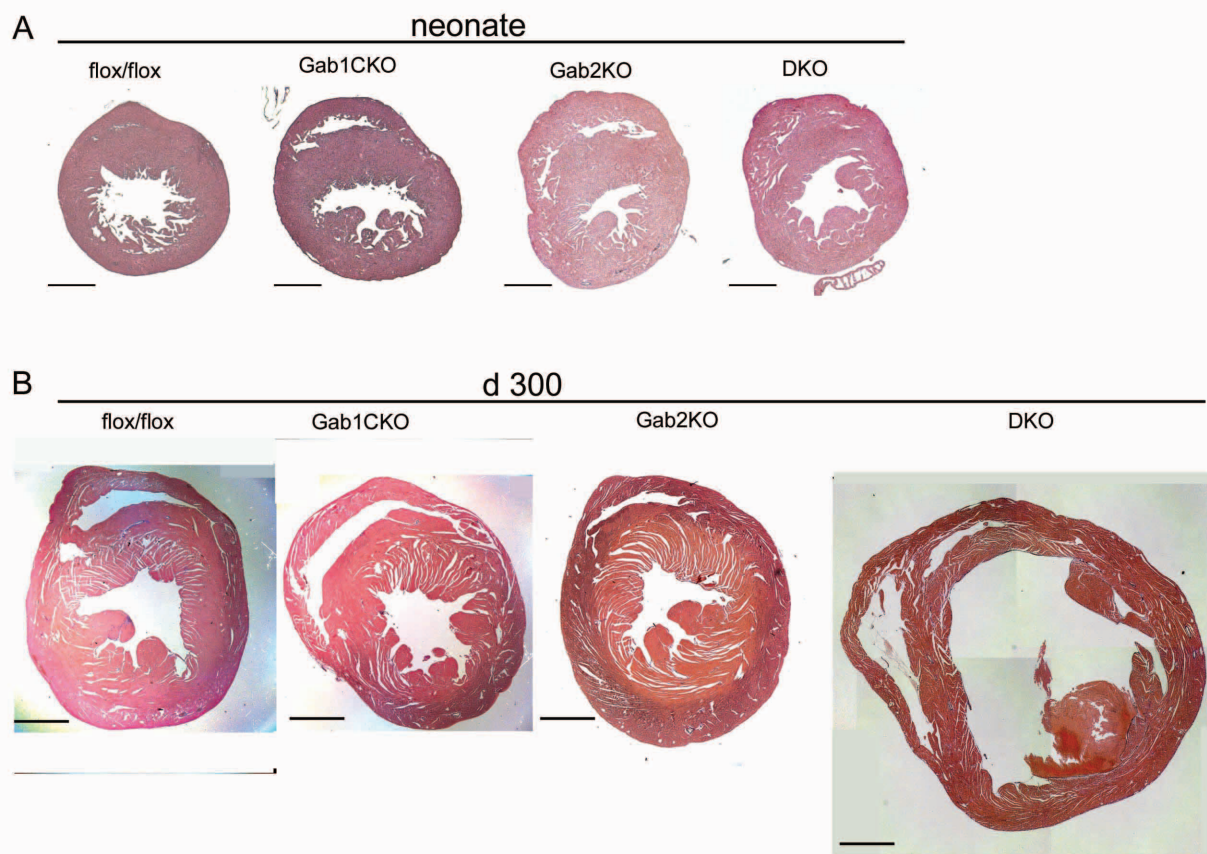




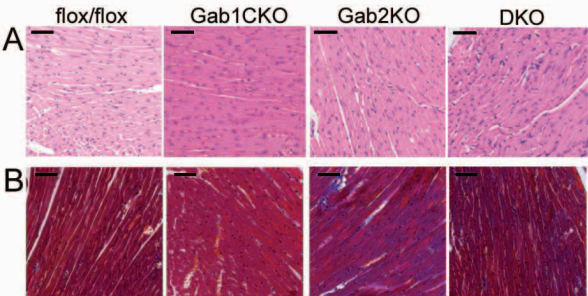
Supplemental Figure 3 Nakaoka et al.



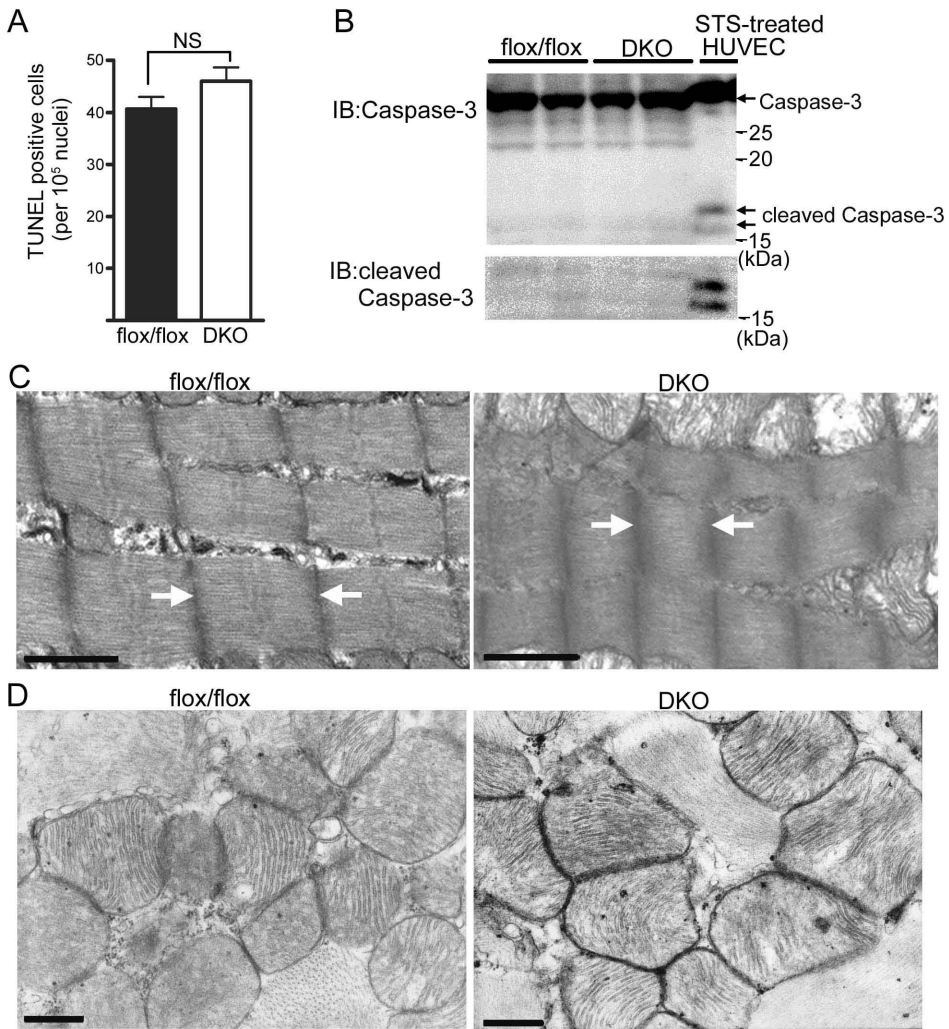
Supplemental Figure 4 Nakaoka et al.



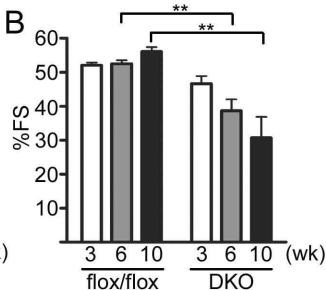
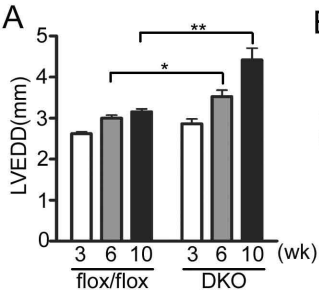
Supplemental Figure 5 Nakaoka et al.



Supplemental Figure 6 Nakaoka et al.



Supplemental Figure 7 Nakaoka et al.



Supplemental Figure 8 Nakaoka et al.

